# A conservative Allen–Cahn equation with a curvature-dependent Lagrange multiplier

Soobin Kwak [a], Junxiang Yang [b], Junseok Kim [a],*

[a] *Department of Mathematics, Korea University, Seoul 02841, Republic of Korea*
[b] *School of Computer Science and Engineering, Sun Yat-sen University, Guangzhou 510275, China*

A R T I C L E   I N F O

A B S T R A C T

In the present study, we propose a novel conservative Allen–Cahn (CAC) equation with a curvature-dependent Lagrange multiplier. The proposed CAC equation has a superior structure-preserving property. Unlike the conventional CAC equations which have motion by mean curvature with area or volume constraint, the proposed model has minimum dynamics of motion by mean curvature and only has smoothing property of interface transition layer. Therefore, it can be utilized as a building block equation for modeling conservative phase-field applications such as two-phase fluid flows. Several computational tests are conducted to confirm the superior performance of the proposed CAC equation in terms of structure-preserving property.

## 1. Introduction

The Allen–Cahn (AC) equation is being studied continuously in various fields [1,2]. In this study, we present a novel conservative Allen–Cahn (CAC) equation. The CAC equations for interface capturing in two-phase fluid flows have recently gained more popularity [3,4]. Traditionally, the Cahn–Hilliard (CH) equation has been applied in modeling interface between two different fluids [5–7]. The most important reasons for getting popularity of using the CAC equation instead of using the CH equation are its simplicity, improved efficiency, and accuracy [8]. The most distinguished difference between the CAC and CH equations is that the former is second-order partial differential equation (PDE) and the latter is fourth-order PDE. Therefore, it is generally more efficient to solve the lower order than the higher order PDEs. There are two most popular CAC equations. The first one is as follows [9,10]:

$$\frac{\partial \phi(\mathbf{x}, t)}{\partial t} = -\frac{F'(\phi(\mathbf{x}, t))}{\epsilon^2} + \Delta \phi(\mathbf{x}, t) + \gamma(t), \tag{1}$$

---

* Corresponding author.
  *E-mail address:* cfdkim@korea.ac.kr (J. Kim).
  *URL:* https://mathematicians.korea.ac.kr/cfdkim/ (J. Kim).

where $\phi(\mathbf{x}, t)$ is the concentration, $F(\phi) = (\phi^2 - 1)^2/4$, $\epsilon$ is a positive constant which controls the thickness of interface transition layer, and $\gamma(t)$ is the time-dependent Lagrange multiplier

$$\gamma(t) = \frac{1}{\epsilon^2} \int_\Omega F'(\phi(\mathbf{x}, t)) \, \mathrm{d}\mathbf{x} \Big/ \int_\Omega \mathrm{d}\mathbf{x}.$$

Note that if $\gamma(t)$ is absent, then Eq. (1) becomes the classical AC equation [11] which models the phase transformation in binary mixtures and the evolution of antiphase boundaries [12]. The second one is as follows [13–17]:

$$\frac{\partial \phi(\mathbf{x}, t)}{\partial t} = -\frac{F'(\phi(\mathbf{x}, t))}{\epsilon^2} + \Delta\phi(\mathbf{x}, t) + \gamma(t)\sqrt{2F(\phi(\mathbf{x}, t))}, \tag{2}$$

where $\gamma(t)\sqrt{2F(\phi(\mathbf{x}, t))}$ is the time-and space-dependent Lagrange multiplier and

$$\gamma(t) = \frac{1}{\epsilon^2} \int_\Omega F'(\phi(\mathbf{x}, t)) \, \mathrm{d}\mathbf{x} \Big/ \int_\Omega \sqrt{2F(\phi(\mathbf{x}, t))} \, \mathrm{d}\mathbf{x}.$$

In [18], the author developed two mass-conserving numerical methods for the AC equation in the mass-conserving space using the mass-projection and energy-dissipation operators. In [19], the author developed a stable and structure-preserving finite difference method for a CAC equation. In [20], the authors presented a new CAC equation and proved the existence, uniqueness, and boundedness property of the solution. The CAC equation with the time-and space-dependent Lagrange multiplier has been applied to multiphase fluid flows [16,21]. However, intrinsically, the conventional CAC models have the property of the motion by mean curvature with constraint. Therefore, if there are initially two drops with different sizes, then the smaller drop is absorbed into the larger drop and eventually disappears. Hence, these CAC models have limitation for applications such as two-phase fluid flows with multiple components with different sizes. To resolve these problems, we propose a novel CAC equation with a curvature-dependent Lagrange multiplier to have a good structure-preserving property. The proposed model has minimum dynamics of motion by mean curvature and only has smoothing property of interface. Therefore, it can be utilized as a building block equation for modeling conservative phase-field applications such as two-phase fluid flows.

This paper is organized as follows. In Section 2, the proposed new CAC equation and its numerical scheme are given. In Section 3, we present some computational tests to confirm the superior performance of the proposed CAC equation in terms of structure-preserving property. Conclusions are drawn in Section 4.

## 2. Proposed CAC equation and its numerical solution algorithm

We propose the following CAC equation with a curvature-dependent Lagrange multiplier :

$$\frac{\partial \phi(\mathbf{x}, t)}{\partial t} = -M \left( \frac{F'(\phi(\mathbf{x}, t))}{\epsilon^2} - \Delta\phi(\mathbf{x}, t) - \gamma(t)\kappa(\phi(\mathbf{x}, t))\sqrt{2F(\phi(\mathbf{x}, t))} \right), \tag{3}$$

where $M$ is the mobility coefficient [22], $\kappa(\phi) = \nabla \cdot (\nabla\phi/|\nabla\phi|)$ is the curvature of the interface, and

$$\gamma(t) = \frac{1}{\epsilon^2} \int_\Omega F'(\phi(\mathbf{x}, t)) \, \mathrm{d}\mathbf{x} \Big/ \int_\Omega \kappa(\phi(\mathbf{x}, t))\sqrt{2F(\phi(\mathbf{x}, t))} \, \mathrm{d}\mathbf{x}.$$

Then, the solution $\phi$ of Eq. (3) satisfies the following equation:

$$\frac{d}{dt} \int_\Omega \phi \, \mathrm{d}\mathbf{x} = \int_\Omega \phi_t \, \mathrm{d}\mathbf{x} = \int_\Omega -M \left[ \frac{F'(\phi)}{\epsilon^2} - \Delta\phi - \gamma(t)\kappa(\phi)\sqrt{2F(\phi)} \right] \mathrm{d}\mathbf{x}$$
$$= -\frac{M}{\epsilon^2} \int_\Omega F'(\phi) \, \mathrm{d}\mathbf{x} + M \int_{\partial\Omega} \mathbf{n} \cdot \nabla\phi \, ds + M\gamma(t) \int_\Omega \kappa(\phi)\sqrt{2F(\phi)} \, \mathrm{d}\mathbf{x} = 0, \tag{4}$$

where we used $\mathbf{n} \cdot \nabla\phi = 0$ on $\partial\Omega$ and $\mathbf{n}$ is the unit normal vector.

Now, we describe a hybrid numerical method for solving the CAC equation on $\Omega = (L_x, R_x) \times (L_y, R_y)$. Let $x_i = L_x + (i - 0.5)h$ for $i = 1, \ldots, N_x$ and $y_j = L_y + (j - 0.5)h$ for $j = 1, \ldots, N_y$. Here, $N_x$ and $N_y$ are positive integers and $h = (R_x - L_x)/N_x = (R_y - L_y)/N_y$. Let $\phi_{ij}^n$ be numerical approximations of $\phi(x_i, y_j, n\tau)$, where $\tau$ is the temporal step size. Using an operator splitting method, we solve the original problem Eq. (3) by solving the following simpler equations [23]:

$$\phi_t(\mathbf{x}, t) = \Delta\phi(\mathbf{x}, t), \tag{5}$$

$$\phi_t(\mathbf{x}, t) = -\frac{F'(\phi(\mathbf{x}, t))}{\epsilon^2}, \tag{6}$$

$$\phi_t(\mathbf{x}, t) = \gamma(t)\kappa(\phi(\mathbf{x}, t))\sqrt{2F(\phi(\mathbf{x}, t))}, \tag{7}$$

where we used $M = 1$. To solve Eq. (5), we use the Fourier-spectral method [24]: For the given data $\{\phi_{ij}^n | i = 1, \ldots, N_x$ and $j = 1, \ldots, N_y\}$, the discrete cosine transform is defined as follows

$$\hat{\phi}_{pq}^n = \alpha_p \beta_q \sum_{i=1}^{N_x} \sum_{j=1}^{N_y} \phi_{ij}^n \cos\frac{(2i-1)(p-1)\pi}{2N_x} \cos\frac{(2j-1)(q-1)\pi}{2N_y}, p = 1, \ldots, N_x \text{ and } q = 1, \ldots, N_y, \tag{8}$$

where $\alpha_1 = \sqrt{1/N_x}$, $\alpha_p = \sqrt{2/N_x}$ if $2 \le p \le N_x$, $\beta_1 = \sqrt{1/N_y}$, and $\beta_q = \sqrt{2/N_y}$ if $2 \le q \le N_y$. For simplicity of exposition, we assume $L_x = L_y = 0$. For the cases of non-zero $L_x$ and $L_y$, please refer to [22]. Let $x_i = (2i - 1)R_x/(2N_x)$, $y_j = (2j - 1)R_y/(2N_y)$, $\xi_p = (p-1)/R_x$, and $\eta_q = (q-1)/R_y$. Then, we can rewrite Eq. (8) as $\hat{\phi}_{pq}^n = \alpha_p \beta_q \sum_{i=1}^{N_x} \sum_{j=1}^{N_y} \phi_{ij}^n \cos(\xi_p \pi x_i) \cos(\eta_q \pi y_j)$. The inverse discrete cosine transform is

$$\phi_{ij}^n = \sum_{p=1}^{N_x} \sum_{q=1}^{N_y} \alpha_p \beta_q \hat{\phi}_{pq}^n \cos(\xi_p \pi x_i) \cos(\eta_q \pi y_j). \tag{9}$$

Let us assume that $\phi(x, y, n\tau) = \sum_{p=1}^{N_x} \sum_{q=1}^{N_y} \alpha_p \beta_q \hat{\phi}_{pq}^n \cos(\xi_p \pi x) \cos(\eta_q \pi y)$. Therefore, the Laplacian operator is defined as

$$\Delta\phi(x, y, n\tau) = \frac{\partial^2 \phi}{\partial x^2}(x, y, n\tau) + \frac{\partial^2 \phi}{\partial y^2}(x, y, n\tau)$$

$$= -\sum_{p=1}^{N_x} \sum_{q=1}^{N_y} (\xi_p \pi)^2 \alpha_p \beta_q \hat{\phi}_{pq}^n \cos(\xi_p \pi x) \cos(\eta_q \pi y) - \sum_{p=1}^{N_x} \sum_{q=1}^{N_y} (\eta_q \pi)^2 \alpha_p \beta_q \hat{\phi}_{pq}^n \cos(\xi_p \pi x) \cos(\eta_q \pi y)$$

$$= -\sum_{p=1}^{N_x} \sum_{q=1}^{N_y} [(\xi_p \pi)^2 + (\eta_q \pi)^2] \alpha_p \beta_q \hat{\phi}_{pq}^n \cos(\xi_p \pi x) \cos(\eta_q \pi y). \tag{10}$$

Using Eqs. (9) and (10), from Eq. (5) we have $d\hat{\phi}_{pq}/dt = -[(\xi_p \pi)^2 + (\eta_q \pi)^2]\hat{\phi}_{pq}$. Then, we have the following solution after time step $\tau$ with the initial condition $\hat{\phi}_{pq}^n$:

$$\hat{\phi}_{pq}^{n+1,1} = \hat{\phi}_{pq}^n e^{-\tau[(\xi_p \pi)^2 + (\eta_q \pi)^2]}. \tag{11}$$

Then, the numerical solution $\phi_{ij}^{n+1,1}$ is obtained using Eqs. (9) and (11), i.e.,

$$\phi_{ij}^{n+1,1} = \sum_{p=1}^{N_x} \sum_{q=1}^{N_y} \alpha_p \beta_q \hat{\phi}_{pq}^{n+1,1} \cos(\xi_p \pi x_i) \cos(\eta_q \pi y_j).$$

Second, Eq. (6) is solved analytically by the method of separation of variables:

$$\phi_{ij}^{n+1,2} = \phi_{ij}^{n+1,1} \bigg/ \sqrt{e^{-\frac{2\tau}{\epsilon^2}} + \left(\phi_{ij}^{n+1,1}\right)^2 \left(1 - e^{-\frac{2\tau}{\epsilon^2}}\right)}.$$
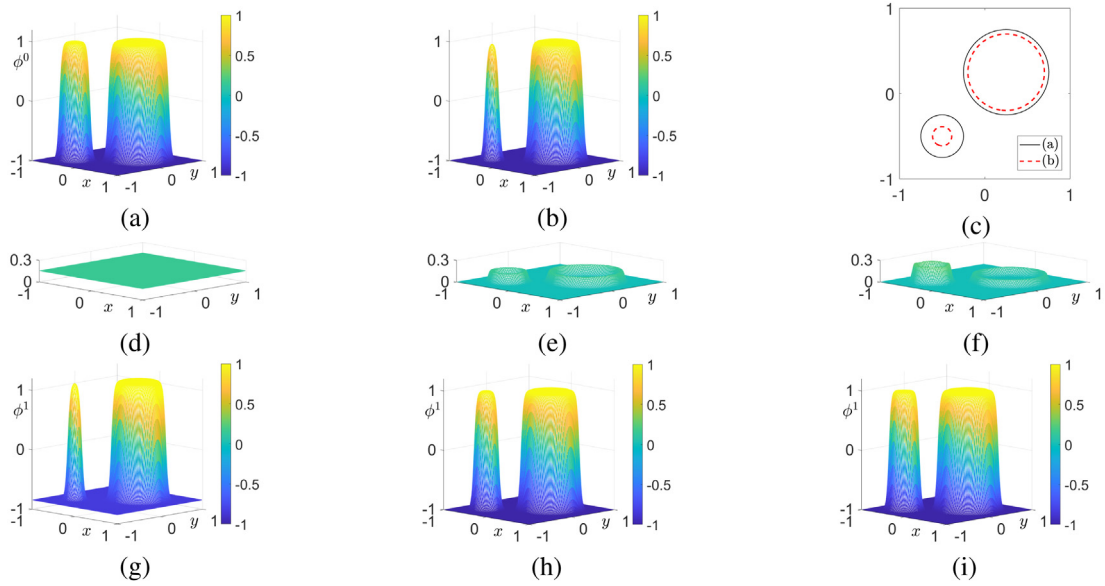
**Fig. 1.** Schematic illustration of conservative algorithms: (a) initial condition $\phi^0$; (b) after solving the AC equation; (c) zero-level contours of (a) and (b); (d), (e), and (f) are conservative corrections $\gamma(t)$, $\gamma(t)\sqrt{2F(\phi)}$, and $\gamma(t)\kappa(\phi)\sqrt{2F(\phi)}$, respectively; (g), (h), and (i) are the solutions $\phi^1$ of the CAC equation with $\gamma(t)$, $\gamma(t)\sqrt{2F(\phi)}$, and $\gamma(t)\kappa(\phi)\sqrt{2F(\phi)}$, respectively.

Third, we discretize Eq. (7) as

$$\frac{\phi_{ij}^{n+1} - \phi_{ij}^{n+1,2}}{\tau} = \gamma^{n+1,2}\kappa(\phi_{ij}^{n+1,2})\sqrt{2F(\phi_{ij}^{n+1,2})}. \tag{12}$$

By Eq. (12), we get $\phi_{ij}^{n+1} = \phi_{ij}^{n+1,2} + \tau\gamma^{n+1,2}\kappa_{ij}^{n+1,2}\sqrt{2F(\phi_{ij}^{n+1,2})}$, then by the property of Eq. (4),

$$\frac{1}{\tau}\left(\sum_{i=1}^{N_x}\sum_{j=1}^{N_y}\phi_{ij}^{n+1} - \sum_{i=1}^{N_x}\sum_{j=1}^{N_y}\phi_{ij}^{n}\right) = 0,$$

$$\sum_{i=1}^{N_x}\sum_{j=1}^{N_y}\phi_{ij}^{0} = \sum_{i=1}^{N_x}\sum_{j=1}^{N_y}\phi_{ij}^{n+1} = \sum_{i=1}^{N_x}\sum_{j=1}^{N_y}\left(\phi_{ij}^{n+1,2} + \tau\gamma^{n+1,2}\kappa_{ij}^{n+1,2}\sqrt{2F(\phi_{ij}^{n+1,2})}\right).$$

Thus, $\gamma^{n+1,2} = \frac{1}{\tau}\sum_{i=1}^{N_x}\sum_{j=1}^{N_y}(\phi_{ij}^{0} - \phi_{ij}^{n+1,2})\Big/\sum_{i=1}^{N_x}\sum_{j=1}^{N_y}\kappa_{ij}^{n+1,2}\sqrt{2F(\phi_{ij}^{n+1,2})}$. Then, the curvature at the cell center is

$$\nabla\cdot\left(\frac{\nabla\phi}{|\nabla\phi|}\right)_{ij} = \frac{1}{2h}\left(\frac{\phi_{x,i+\frac{1}{2},j+\frac{1}{2}} + \phi_{y,i+\frac{1}{2},j+\frac{1}{2}}}{|\nabla\phi_{i+\frac{1}{2},j+\frac{1}{2}}|} + \frac{\phi_{x,i+\frac{1}{2},j-\frac{1}{2}} - \phi_{y,i+\frac{1}{2},j-\frac{1}{2}}}{|\nabla\phi_{i+\frac{1}{2},j-\frac{1}{2}}|}\right.$$
$$\left. - \frac{\phi_{x,i-\frac{1}{2},j+\frac{1}{2}} - \phi_{y,i-\frac{1}{2},j+\frac{1}{2}}}{|\nabla\phi_{i-\frac{1}{2},j+\frac{1}{2}}|} - \frac{\phi_{x,i-\frac{1}{2},j-\frac{1}{2}} + \phi_{yi-\frac{1}{2},j-\frac{1}{2}}}{|\nabla\phi_{i-\frac{1}{2},j-\frac{1}{2}}|}\right).$$

To avoid numerical singularity when $|\nabla\phi|$ is close to zero, we set $\kappa_{ij} = 0$ outside of the interface, i.e., $|\phi_{ij}| > 0.98$.

Let us consider the basic mechanism of the proposed model. Fig. 1 is a step-by-step schematic illustration of the algorithms for the three different CAC Eqs. (1), (2), and (3). Fig. 1(a) shows an initial condition $\phi^0$ consisting of two different sized disks. Fig. 1(b) is the numerical solution after solving the AC equation,

i.e., steps (5) and (6). The smaller disk shrinks more than the larger disk because of the property of motion by mean curvature. We can observe this phenomenon in Fig. 1(c), which is zero-level contours of Figs. 1(a) and (b). Figs. 1(d), (e), and (f) are conservative correction $\gamma(t)$, $\gamma(t)\sqrt{2F(\phi)}$, and $\gamma(t)\kappa(\phi)\sqrt{2F(\phi)}$, respectively. Unlike the conventional mass correction by shifting a constant or smoothed Dirac delta function like profile across the interface transition layer, the proposed mass correction scheme has curvature-dependent profiles as shown in Fig. 1(f). Figs. 1(g), (h), and (i) are the solutions $\phi^1$ of the CAC equation with $\gamma(t)$, $\gamma(t)\sqrt{2F(\phi)}$, and $\gamma(t)\kappa(\phi)\sqrt{2F(\phi)}$, respectively. Therefore, the main mechanism of the proposed model is that we correct the mass loss from the motion by mean curvature part using curvature-dependent Lagrange multiplier.

## 3. Computational tests

Now, we present some computational tests to confirm the superior performance of the proposed CAC equation. Let us use the notation, $\epsilon_m = hm/[2\sqrt{2}\tanh^{-1}(0.9)]$, where $h$ is grid size and $m$ is a positive integer. We have approximately $hm$ transition layer across interface, see [25] for a more detailed explanation of $\epsilon_m$. Unless otherwise indicated, we shall use $\epsilon = \epsilon_5$.

### 3.1. Structure preserving property

Now, we perform a numerical test which highlights the different dynamics of the proposed CAC equation from the other two conventional CAC equations. Let us consider the following initial condition on $\Omega = (-2, 2) \times (-2, 2)$:

$$\phi(x, y, 0) = 1 + \tanh\left(\frac{0.5 - \sqrt{(x+1)^2 + (y+1)^2}}{\sqrt{2}\epsilon}\right) + \tanh\left(\frac{1 - \sqrt{(x-0.5)^2 + (y-0.5)^2}}{\sqrt{2}\epsilon}\right).$$

The parameters used are $h = 0.0625$ and $\tau = 0.1h^2$. From the top and middle rows in Fig. 2, as schematically illustrated in Fig. 1, in the cases of the Lagrange multipliers $\gamma(t)$ and $\gamma(t)\sqrt{2F(\phi)}$, the smaller disk shrinks and the larger disk grows; and eventually one single disk remains. However, in the case of the proposed Lagrange multiplier $\gamma(t)\kappa(\phi)\sqrt{2F(\phi)}$ (the bottom row), the initial shapes are preserved as time evolves. In addition, Fig. 2(d) shows the temporal evolution of the average concentration $\phi_{ave}$ and $\|\phi^0 - \phi^n\|_2/\|\phi^0\|_2$, where $\|\cdot\|_2$ is the discrete $l_2$-norm. We can observe the average concentration is constant for the three cases. However, only the proposed preserves well the relative deviation from the initial profiles, i.e., $\|\phi^0 - \phi^n\|_2/\|\phi^0\|_2$ is very small.

To further confirm the performance of the proposed CAC equation, let us consider more complex shape on $\Omega = (-2, 2) \times (-2, 2)$ as shown in Fig. 3(a):

$$\phi(x, y, 0) = \tanh\left(\left(2\left(\frac{x^2 - y^2}{x^2 + y^2}\right)^3 - 1.5\left(\frac{x^2 - y^2}{x^2 + y^2}\right) + 1.3 - \sqrt{x^2 + y^2}\right)\Big/(\sqrt{2}\epsilon)\right).$$

Here, we use $h = 1/32$ and $\tau = 0.1h^2$. Fig. 3(b), (c), and (d) show the computational results at $t = 1000\tau$ with the three different Lagrange multipliers $\gamma(t)$, $\gamma(t)\sqrt{2F(\phi)}$, and $\gamma(t)\kappa(\phi)\sqrt{2F(\phi)}$, respectively. Fig. 3(e) and (f) are the zero level contours of $\phi$ at $t = 1000\tau$ and equilibrium state, respectively. In this study, the numerical equilibrium state is defined if $\|\phi^{n+1} - \phi^n\|_2 < 10^{-5}$. Numerical solutions with $\gamma(t)$, $\gamma(t)\sqrt{2F(\phi)}$, and $\gamma(t)\kappa(\phi)\sqrt{2F(\phi)}$ reached the equilibrium state at $n = 3109$, $3128$, and $4387$, respectively. Both the results from the conventional CAC equations have circular shapes because of the motion by mean curvature with mass constraint. However, the proposed CAC equation preserves the original complex shape as time evolves. In addition, 3(g) displays the temporal evolution of the maximum norm of each term in the proposed equation, which indicates that the three terms balance each other.
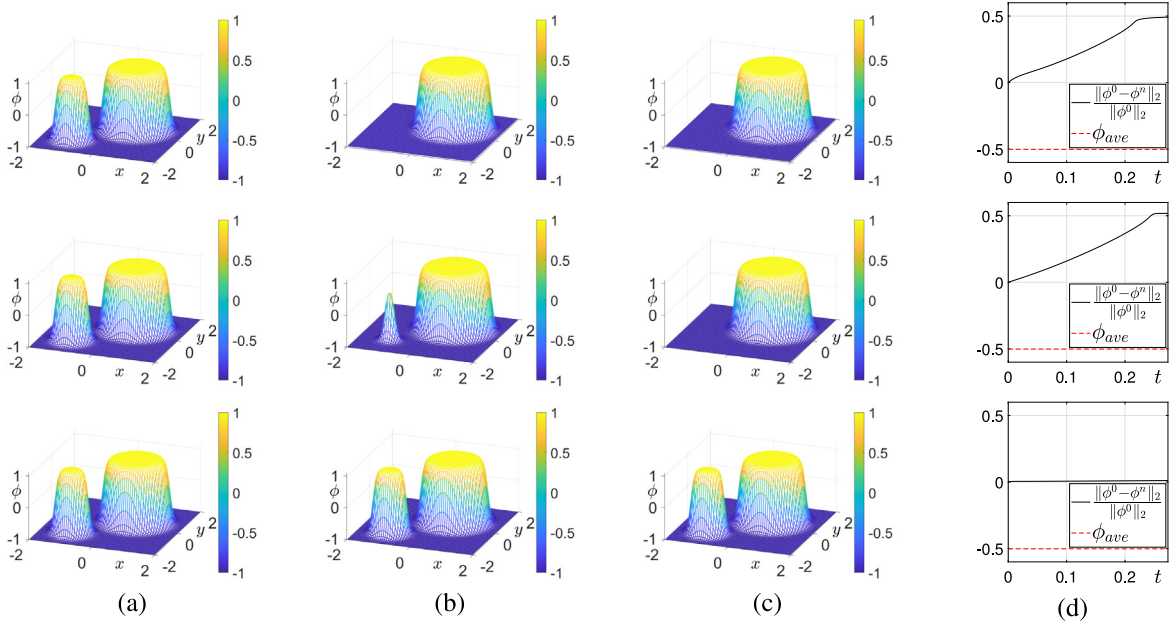
**Fig. 2.** Temporal evolution of the numerical results with different Lagrange multipliers: $\gamma(t)$, $\gamma(t)\sqrt{2F(\phi)}$, and $\gamma(t)\kappa(\phi)\sqrt{2F(\phi)}$ from top to bottom rows, respectively. (a), (b), and (c) are the results at times $t = 0$, $600\tau$, and $700\tau$, respectively. (d) is the temporal evolution of the average concentration $\phi_{ave}$ and $\|\phi^0 - \phi^n\|_2 / \|\phi^0\|_2$.
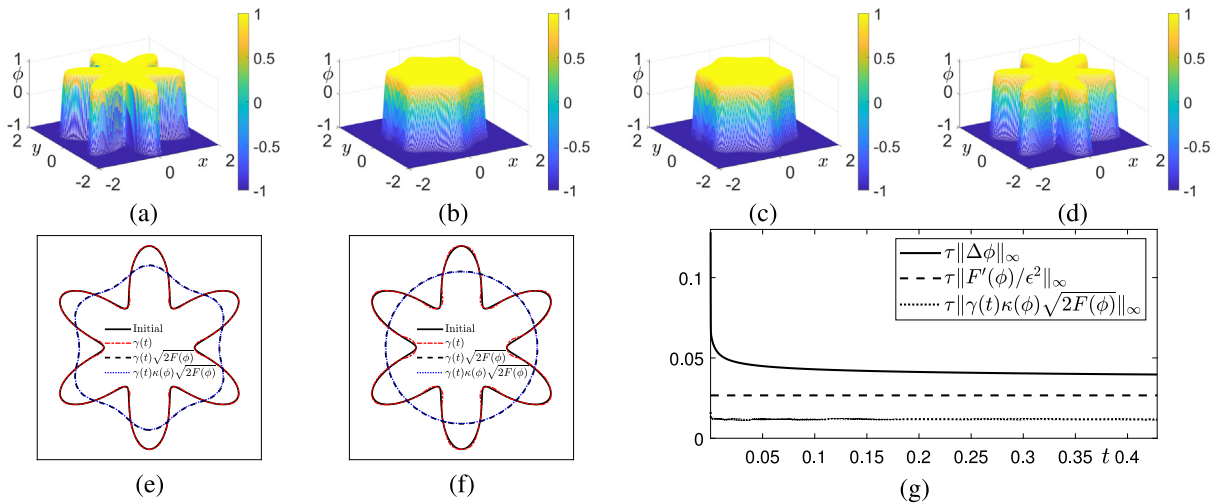


**Fig. 3.** (a) is the initial condition. (b), (c), and (d) are the snapshots of the numerical results at time $t = 1000\tau$ with different Lagrange multipliers: $\gamma(t)$, $\gamma(t)\sqrt{2F(\phi)}$, and $\gamma(t)\kappa(\phi)\sqrt{2F(\phi)}$, respectively. (e) is the zero-level contours of (b)–(d). (f) is the zero-level contours of $\phi$ at equilibrium state. (g) is the temporal evolution of the maximum norm of each term in the proposed equation.

## 3.2. Droplet deformation in swirling flow

Next, we consider the droplet deformation under the background swirling flow. The governing equation is as follows:

$$\frac{\partial \phi(\mathbf{x}, t)}{\partial t} + \nabla \cdot [\phi(\mathbf{x}, t)\mathbf{u}(\mathbf{x})] = -\frac{F'(\phi(\mathbf{x}, t))}{\epsilon^2} + \Delta\phi(\mathbf{x}, t) + \gamma(t)\kappa(\phi(\mathbf{x}, t))\sqrt{2F(\phi(\mathbf{x}, t))}. \tag{13}$$
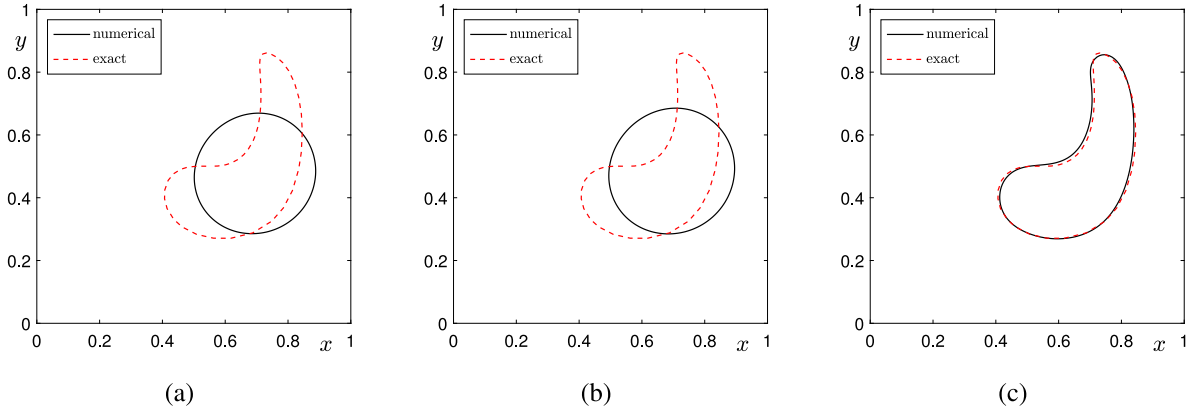
**Fig. 4.** (a), (b), and (c) are droplet deformations under the background swirling flow with $\gamma(t)$, $\gamma(t)\sqrt{2F(\phi)}$, and $\gamma(t)\kappa(\phi)\sqrt{2F(\phi)}$ at $t = 0.195$, respectively. The numerical and exact solutions are represented by the black solid and red dotted lines, respectively.

The advection term in Eq. (13) is solved by the finite difference method.

$$\frac{\phi_{ij}^{n+1} - \phi_{ij}^n}{\tau} = -\frac{(\phi_{i+1,j}^n + \phi_{ij}^n)u_{i+\frac{1}{2},j} - (\phi_{ij}^n + \phi_{i-1,j}^n)u_{i-\frac{1}{2},j}}{2h} + \frac{(\phi_{i,j+1}^n + \phi_{ij}^n)v_{i,j+\frac{1}{2}} - (\phi_{ij}^n + \phi_{i,j-1}^n)v_{i,j-\frac{1}{2}}}{2h}.$$

Here, $u(x, y) = -2.5\sin^2(\pi x)\sin(2\pi y)$ and $v(x, y) = 2.5\sin^2(\pi y)\sin(2\pi x)$. The initial condition is defined on $\Omega = (0, 1) \times (0, 1)$ as $\phi(x, y, 0) = \tanh\left(\frac{0.2 - \sqrt{(x-0.5)^2 + (y-0.7)^2}}{\sqrt{2}\epsilon}\right)$. The parameters used are $h = 1/128$, $\tau = 0.2h^2$, and $\epsilon = \epsilon_8$. Fig. 4(a), (b), and (c) are the snapshots of interfacial position using $\gamma(t)$, $\gamma(t)\sqrt{2F(\phi)}$, and $\gamma(t)\kappa\sqrt{2F(\phi)}$, respectively. It can be observed that the numerical solution obtained by the proposed model shows good agreement with the exact reference solution.

### 3.3. Rotation of a Zalesak's disk

For a further benchmark test, we consider the rotation of a Zalesak's disk, which has been widely used in various interface capturing methods [26,27]. The initial state on $\Omega = (0, 1) \times (0, 1)$ is shown in Fig. 5(a). The background velocity field $u(x, y) = 600(y - 0.5)$, $v(x, y) = -600(x - 0.5)$, $h = 1/256$, $\tau = 0.01h^2$, and $\epsilon = \epsilon_8$ are used. By using the initial interfacial position and background velocity field, the exact result is computed by using the second-order accurate modified Euler method [28]. In Figs. 5(a), (b), and (c), we plot the snapshots of the numerical results with $\gamma(t)$, $\gamma(t)\sqrt{2F(\phi)}$, and $\gamma(t)\kappa\sqrt{2F(\phi)}$ at times $t = 0$, 0.0024, and 0.0043. As we can observe, the computational result from the proposed model preserves well the initial shape.

### 4. Conclusions

In this paper, we proposed a novel CAC equation with a curvature-dependent Lagrange multiplier. The proposed CAC equation has a superior structure-preserving property. Unlike the conventional CAC equations which have motion by mean curvature with area or volume constraint, the proposed model has minimum dynamics of motion by mean curvature and only have smoothing property of interface transition layer. Therefore, it can be utilized as a building block equation for modeling conservative phase-field applications such as two-phase fluid flows. We presented several numerical experiments to demonstrate the superior performance of the proposed CAC equation in terms of structure-preserving property. As future research directions, we will extend the proposed model to vector-valued CAC system [29] and multi-phase fluid flows with surface tension [30,31].
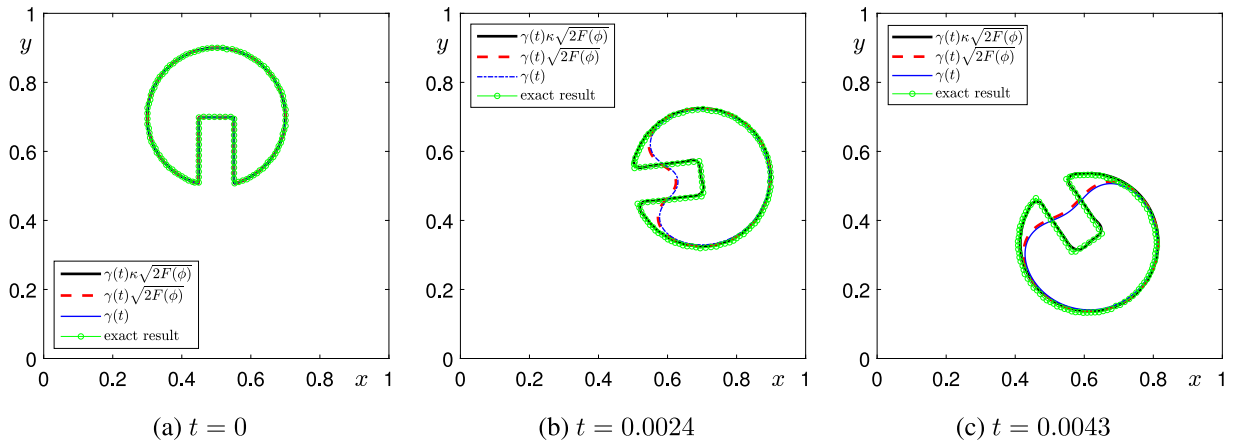
**Fig. 5.** Rotation of a Zalesak's disk with $\gamma(t)$, $\gamma(t)\sqrt{2F(\phi)}$, and $\gamma(t)\kappa(\phi)\sqrt{2F(\phi)}$. The computational moments are shown under each figure.

## Acknowledgments

## References

[1] J. Feng, Y. Zhou, T. Hou, A maximum-principle preserving and unconditionally energy-stable linear second-order finite difference scheme for Allen–Cahn equations, Appl. Math. Lett. 118 (2021) 107179.

[2] J. Zhao, A revisit of the energy quadratization method with a relaxation technique, Appl. Math. Lett. 120 (2021) 107331.

[3] J. Li, L. Ju, Y. Cai, X. Feng, Unconditionally maximum bound principle preserving linear schemes for the conservative Allen–Cahn equation with nonlocal constraint, J. Sci. Comput. 87 (3) (2021) 1–32.

[4] M. Sugimoto, Y. Sawada, M. Kaneda, K. Suga, Consistent evaporation formulation for the phase-field lattice Boltzmann method, Phys. Rev. E 103 (5) (2021) 053307.

[5] L. Chen, J. Zhao, A novel second-order linear scheme for the Cahn–Hilliard–Navier–Stokes equations, J. Comput. Phys. 423 (2021) 109782.

[6] C. Liu, F. Frank, C. Thiele, F.O. Alpak, S. Berg, W. Chapman, et al., An efficient numerical algorithm for solving viscosity contrast Cahn–Hilliard–Navier–Stokes system in porous media, J. Comput. Phys. 400 (2020) 108948.

[7] N. Adam, F. Franke, S. Aland, A simple parallel solution method for the Navier–Stokes Cahn–Hilliard equations, Mathematics 8 (8) (2020) 1224.

[8] A. Begmohammadi, R. Haghani-Hassan-Abadi, A. Fakhari, D. Bolster, Study of phase-field lattice Boltzmann models based on the conservative Allen–Cahn equation, Phys. Rev. E 102 (2) (2020) 023305.

[9] J. Rubinstein, P. Sternberg, Nonlocal reaction–diffusion equations and nucleation, IMA J. Appl. Math. 48 (3) (1992) 249–264.

[10] B. Xia, Y. Li, Z. Li, Second-order unconditionally stable direct methods for Allen–Cahn and conservative Allen–Cahn equations on surfaces, Mathematics 8 (9) (2020) 1486.

[11] S.M. Allen, J.W. Cahn, A microscopic theory for antiphase boundary motion and its application to antiphase domain coarsening, Acta Metall. 27 (1979) 1085–1095.

[12] H. Li, Z. Song, J. Hu, Numerical analysis of a second-order IPDGFE method for the Allen–Cahn equation and the curvature-driven geometric flow, Comput. Math. Appl. 86 (2021) 49–62.

[13] M. Brassel, E. Bretin, A modified phase field approximation for mean curvature flow with conservation of the volume, Math. Methods Appl. Sci. 34 (10) (2011) 1157–1180.

[14] Z. Weng, Q. Zhuang, Numerical approximation of the conservative Allen–Cahn equation by operator splitting method, Math. Methods Appl. Sci. 40 (12) (2017) 4462–4480.

[15] Z. Huang, G. Lin, A.M. Ardekani, Consistent and conservative scheme for incompressible two-phase flows using the conservative Allen–Cahn model, J. Comput. Phys. 420 (2020) 109718.

[16] V. Joshi, R.K. Jaiman, A positivity preserving and conservative variational scheme for phase-field modeling of two-phase flows, J. Comput. Phys. 360 (2018) 137–166.

[17] P.H. Chiu, A coupled phase field framework for solving incompressible two-phase flows, J. Comput. Phys. 392 (2019) 115–140.

[18] D. Lee, The numerical solutions for the energy-dissipative and mass-conservative Allen–Cahn equation, Comput. Math. Appl. 80 (1) (2020) 263–284.
[19] M. Okumura, A stable and structure-preserving scheme for a non-local Allen–Cahn equation, Jpn J. Ind. Appl. Math. 35 (3) (2018) 1245–1281.
[20] D. Lee, Y. Kim, Novel mass-conserving Allen–Cahn equation for the boundedness of an order parameter, Commun. Nonlinear Sci. Numer. Simul. 85 (2020) 105224.
[21] X. Mao, V. Joshi, R. Jaiman, A variational interface-preserving and conservative phase-field method for the surface tension effect in two-phase flows, J. Comput. Phys. 433 (2021) 110166.
[22] Q. Hong, Y. Gong, J. Zhao, Q. Wang, Arbitrarily high order structure-preserving algorithms for the Allen–Cahn model with a nonlocal constraint, Appl. Math. Lett. 170 (2021) 321–339.
[23] Z. Weng, L. Tang, Analysis of the operator splitting scheme for the Allen–Cahn equation, Numer. Heat. Tranf. B-Fundam. 70 (5) (2016) 472–483.
[24] H.G. Lee, J.Y. Lee, A semi-analytical Fourier spectral method for the Allen–Cahn equation, Comput. Math. Appl. 68 (3) (2014) 174–184.
[25] J. Kim, Phase-field models for multi-component fluid flows, Commun. Comput. Phys. 12 (3) (2012) 613–661.
[26] D. Kim, C.B. Ivey, F.H. Ham, L.G. Bravo, An efficient high-resolution Volume-of-Fluid method with low numerical diffusion on unstructured grids, J. Comput. Phys. 446 (2021) 110606.
[27] M. Gutforth, P.T. Barton, N. Nikiforakis, An efficient moment-of-fluid interface tracking method, Comput. Fluids 224 (2021) 104964.
[28] J. Yang, Y. Li, C. Lee, J. Kim, Conservatie Allen–Cahn equation with a nonstandard variable mobility, Acta Mech. 231 (2020) 561–576.
[29] J. Kim, H.G. Lee, A new conservative vector-valued Allen–Cahn equation and its fast numerical method, Comput. Phys. Comm. 221 (2017) 102–108.
[30] S. Aihara, T. Takaki, N. Takada, Multi-phase-field modeling using a conservative Allen–Cahn equation for multiphase flow, Comput. Fluids 178 (2019) 141–151.
[31] L. Zheng, S. Zheng, Q. Zhai, Multiphase flows of N immiscible incompressible fluids: Conservative Allen–Cahn equation and lattice Boltzmann equation method, Phys. Rev. E 101 (1) (2020) 013305.